Certifying Non-Classicality and Non-Gaussianity Through Optical Parametric Amplification

Mahmoud Kalash,[1,2,*] M. H. M. Passos,[1,4] Éva Rácz,[3] László Ruppert,[3] Radim Filip,[3] and Maria V. Chekhova[1,2,†]

[1]*Max Planck Institute for the Science of Light, Staudtstraße 2, 91058, Erlangen, Germany*
[2]*Friedrich-Alexander-Universität Erlangen–Nürnberg, Staudtstraße 7/B2, 91058, Erlangen, Germany*
[3]*Department of Optics, Palacký University, 17. listopadu 1192/12, 779 00 Olomouc, Czech Republic*
[4]*Centro Brasileiro de Pesquisas Físicas, Rua Dr. Xavier Sigaud, 150, Urca, Rio de Janeiro, 22290-180, RJ, Brazil*

(Received 20 October 2025; accepted 3 June 2026; published 30 July 2026)

Non-Gaussian states of light are essential for numerous quantum information protocols; thus, certifying non-Gaussianity (NG) is crucial. Full quantum state tomography, commonly used for this purpose, is complicated and yields inconclusive results for strongly mixed states. Certifying NG through directly measurable parameters is a simpler alternative, typically achieved by measuring photon-number probabilities—either directly, using photon-number resolving detectors, or through Hanbury Brown-Twiss type measurements with single-photon detectors. Here, we demonstrate, theoretically and experimentally, that phase-sensitive optical parametric amplification (OPA), followed by conventional intensity detection, can effectively replace this approach. Our proposed witness relies on the mean photon number (relative to that produced by the amplifier without any input) and the second-order correlation function after OPA. Both can be directly obtained from the measured amplified intensity and are invariant to detection losses. The method therefore requires neither photon-number resolution nor high detection efficiency. In a proof-of-principle experiment, we successfully certify the quantum NG of a heralded quasi-single-photon state. Since OPA is a broadband and multimode process, our method provides a foundation for developing high-dimensional quantum technologies utilizing broadband multimode non-Gaussian states.

DOI: 10.1103/j68x-skmn

I. INTRODUCTION

Nonclassical states of light, i.e., states that cannot be represented as mixtures of coherent states, are indispensable for quantum photonics. But several quantum information protocols, such as, for instance, entanglement distillation or quantum error correction, require even more "exotic" nonclassical resources, namely quantum non-Gaussian states [1–6]—those which cannot be represented even as mixtures of states with Gaussian Wigner functions.

While there is no experimentally testable definition of nonclassicality (NC) or non-Gaussianity (NG), there are several sufficient conditions (witnesses) for them. Nonclassicality, for instance, can be experimentally certified through anti-bunching [7]. Certifying a state being non-Gaussian is less trivial. This may be done through the measurement of the Wigner function: its negativity [8,9] is a direct evidence of non-Gaussianity [10–12]. However, for mixed non-Gaussian states, which are commonly encountered in practice, the Wigner function can be positive [13–16].

To certify the quantum NG or NC of states whose properties are not apparent through the Wigner function, other measurements are needed. One possibility is measuring the value of the Wigner function at the origin by a photon-parity detector, together with the mean photon number [17]. Another, broader used witness, is based on the photon-number (Fock) probabilities of a state [13,14,18–20].

Figure 1(a) shows how NC and NG can be certified through the probabilities of zero-photon (p_0) and single-photon (p_1) events: for classical states and a fixed probability p_0, the probability p_1 cannot exceed a certain limit, which is a function of p_0 (the dotted line). A similar limit (blue solid line) cannot be exceeded for Gaussian states [13,14,20]. If p_1 exceeds one of these limits, we can certify the NC or NG of the state. In particular, the green and blue areas in Fig. 1(a) cannot be reached by classical states, and the green area cannot be accessed through any mixture of Gaussian states either (for details, see Appendix F). The gray hatched areas in Fig. 1(a) correspond to non-physical states ($p_0 + p_1 > 1$). Experimentally, p_0 and p_1 can be measured through the

*Contact author: mahmoud.kalash@mpl.mpg.de
†Contact author: maria.chekhova@mpl.mpg.de

Published by the American Physical Society under the terms of the Creative Commons Attribution 4.0 International license. Further distribution of this work must maintain attribution to the author(s) and the published article's title, journal citation, and DOI. Open access publication funded by Max Planck Society.

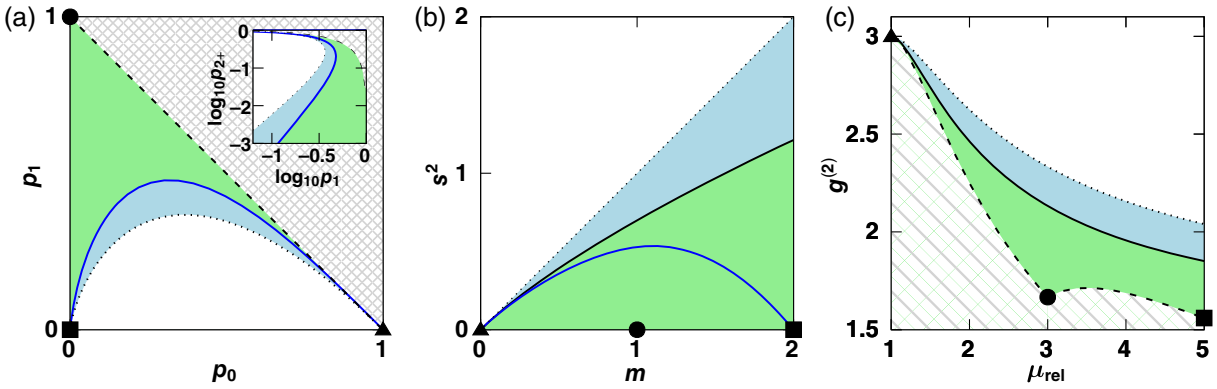


FIG. 1. (a) Non-Gaussianity (NG) and nonclassicality (NC) witnesses in terms of vacuum (p_0) and single-photon (p_1) probabilities [13]. The area above the dotted line (blue and green parts) is not accessible by classical states, while the green area above the blue line is not accessible by Gaussian states. The cross-hatched area is non-physical. Inset: the same criteria in terms of single-photon (p_1) and higher photon-number (p_{2+}) probabilities. (b) The NG witness in terms of photon-number mean m and variance s^2 (black line). The blue line shows the photon-number probability-based NG witness converted to m, s^2 variables. The dotted line is the boundary of the anti-bunching nonclassicality witness $g^{(2)} < 1$. (c) NG and NC witnesses in terms of the post-amplification second-order correlation function $g^{(2)}$ and mean photon number relative to the one of the amplified vacuum $\mu_{\rm rel}$, applicable to phase-independent states. The dashed area is where phase-independent states cannot reach. The dashed line for $\mu_{\rm rel} \in (1, 3)$ corresponds to different input mixtures of a vacuum and a single photon and for $\mu_{\rm rel} \in (3, 5)$, to input mixtures of single-photon and two-photon states. White areas in all panels correspond to points that classical states can reach. The black triangular, circular, and square markers correspond to Fock states $|0\rangle$, $|1\rangle$, and $|2\rangle$, respectively.

standard Hanbury Brown-Twiss (HBT) setup [14,21] with single-photon detectors (SPDs), as long as the mean photon number is much less than 1. Applying a similar method to brighter states requires detectors with photon-number resolution or multiple single-photon detectors, both options being resource-consuming.

This problem, as it turns out, can be overcome through the use of phase-sensitive optical parametric amplification (OPA)—a powerful tool for direct intensity-based quantum state detection. It increases the efficiency of direct detection [22], even at the single-photon level [23]. Additionally, it improves quantum state reconstruction [24], and enables quantum state characterization without homodyne detection, through intensity detection only [25–29], including the simultaneous measurement of squeezing in multiple eigenmodes [30]. It is therefore desirable to formulate NC and NG witnesses directly in terms of intensity observables, whose direct detection may be assisted by phase-sensitive optical parametric amplification.

Indeed, Fig. 1(b) shows the NG witness involving only the mean photon number m and photon-number variance s^2 (for the detailed proof, see [31]), similar to the sub-Poissonian witness of NC. The NG is certified whenever the variance is below the black line, which is a stricter condition than sub-Poissonian behavior (below the dashed line), but much less strict than the earlier NG condition (blue line). Still, the direct application of this witness would require photon-number measurements in the mesoscopic range, which is technically difficult. Furthermore, in the presence of losses, the estimation of s^2 is not very precise in practice. Therefore, the direct use of the (s^2, m) witness for realistic mesoscopic states requires efficient detection.

To overcome both these limitations, we use phase-sensitive amplification followed by direct intensity detection and reformulate the NC and NG conditions in terms of post-amplification observables: the mean intensity relative to the OPA noise and the second-order intensity correlation function [32]. Importantly, unlike the methods based on photon-number probabilities [Fig. 1(a)] or the direct application of the mean-variance witness [Fig. 1(b)], our experimental approach is based on intensity variables, measurable with conventional intensity detectors and invariant to the loss after the OPA, and therefore requires neither photon-number resolution nor a high detection efficiency.

To prove the principle, we seed an OPA with a heralded quasi-single-photon state and study the photon-number statistics. Although the full photon-number distribution of the amplified state generally may be used for state tomography [28], in our case, it does not suffice to reveal NG. Due to the significant degradation of the input single photon and multiphoton effects stemming from the conditional preparation of the state, no Wigner negativity is present, a situation frequently observed under realistic experimental conditions. We show, however, that our witness based on the mean photon number and second-order correlation function is robust enough to certify NG even for highly degraded states. This is demonstrated by tracking the witness as we increase the brightness of the input state, revealing a gradual transition from certified

NG to certified NC only, and eventually to inconclusive result as higher-order photon contributions arise. The results align well with those obtained from the standard coincidence measurements for faint heralded single-photon states and extend to brighter states, where single-photon detectors become unusable.

II. PHOTON-NUMBER STATISTICS OF AMPLIFIED QUANTUM STATES

When characterizing a state at the input of an OPA, one parameter to consider is the mean photon number after amplification, $\mu \equiv \langle \hat{N} \rangle$, with $\hat{N} = \hat{a}^\dagger \hat{a}$ being the photon number operator and $\hat{a}^\dagger$ ($\hat{a}$) the photon creation (annihilation) operator, respectively. Using the Bogoliubov transformation,

$$\hat{a} = \hat{a}_0 \cosh G + \hat{a}_0^\dagger \sinh G, \tag{1}$$

with the parametric gain G and input operators $\hat{a}_0, \hat{a}_0^\dagger$ (which, in terms of quadratures, is equivalent to $\hat{x}_0 \to e^G \hat{x}_0$ and $\hat{p}_0 \to e^{-G} \hat{p}_0$), we can evaluate μ for various input states. For example, when the OPA is seeded with a vacuum, a thermal state with the mean photon number $\bar{n}$, and a Fock state $|n\rangle$, the post-amplification mean photon numbers are, respectively, $\mu_{\text{vac}} = \sinh^2 G$, $\mu_{\text{th}} = \bar{n} \cdot \cosh 2G + \sinh^2 G$, and $\mu_{|n\rangle} = n \cdot \cosh 2G + \sinh^2 G$ [33]. Although sensitive to the input energy, the latter two cases demonstrate that the mean photon number after amplification is, on its own, not suitable to discriminate between different types of states: μ is the same for thermal or Fock inputs when $\bar{n} = n$.

On the other hand, the normalized second-order correlation function $g^{(2)}(0) = \frac{\langle \hat{a}^\dagger \hat{a}^\dagger \hat{a} \hat{a} \rangle}{\langle \hat{a}^\dagger \hat{a} \rangle \langle \hat{a}^\dagger \hat{a} \rangle}$, here denoted for simplicity $g^{(2)}$, has proven to be a highly effective tool for characterizing the intensity statistics of an electric field, thereby providing insights into the nature of photon streams and their statistical properties [34]. For instance, $g^{(2)} = 1$ corresponds to coherent (Poissonian) statistics, while $g^{(2)} = 2$ indicates thermal (super-Poissonian) statistics. To illustrate how $g^{(2)}$ reflects the input state NG, consider amplification of different states. At high amplification gain, vacuum and thermal states both yield $g^{(2)} \approx 3$, due to strong quadrature anti-squeezing causing large intensity fluctuations [33]. However, amplified Fock states yield significantly lower $g^{(2)}$ (≤ 1.66 for $n \geq 1$), which clearly indicates the sensitivity of $g^{(2)}$ to the NG of the input states.

III. NON-CLASSICALITY AND NON-GAUSSIANITY WITNESSES THROUGH OPTICAL PARAMETRIC AMPLIFICATION

In the current method, we measure the intensity and its moments after the amplification of a state. Instead of the anti-bunching NC witness [$g^{(2)} < 1$, Fig. 1(b)], we construct similar NC and NG witnesses in terms of the mean photon number μ and the normalized second-order correlation $g^{(2)}$ after amplification. To make the analysis independent of the detection efficiency and, additionally, of the parametric gain G, we define the normalized mean photon number $\mu_{\text{rel}} \equiv \mu/\mu_{\text{vac}}$, where $\mu_{\text{vac}} = \sinh^2 G$ is the mean photon number for amplified vacuum, i.e., the noise of the OPA. Note that if the detection efficiency after amplification is denoted by η_{det}, the corresponding mean intensities become $\mu' = \eta_{\text{det}}\mu$ and $\mu'_{\text{vac}} = \eta_{\text{det}}\mu_{\text{vac}}$, so μ_{rel} remains unchanged, as well as $g^{(2)}$, of course.

We plotted the boundaries of these new single-mode witnesses with dotted (NC) and solid (NG) black lines in Fig. 1(c) (see Appendix F for derivation). The NC boundary can be given by

$$g^{(2)}_{\text{NC}}(\mu_{\text{rel}}) = \frac{3}{2} + \frac{3}{\mu_{\text{rel}}} - \frac{3}{2\mu_{\text{rel}}^2}, \tag{2}$$

and the NG boundary is most compactly provided as a parametric curve

$$\begin{aligned} \tilde{\mu}_{\text{rel}}(r) &= e^r \cosh 2r, \\ \tilde{g}^{(2)}(r) &= 3 - 3 \cdot \frac{\sinh^2 r \cdot \left(\sinh 2r + 1\right)}{\cosh^2 2r}, \end{aligned} \tag{3}$$

with $r \geq 0$. Witnessing the fact that a state cannot be represented by mixtures of coherent states (NC) or by mixtures of Gaussian states (NG) requires that the point $(\mu_{\text{rel}}, g^{(2)})$ lies beneath the parametric curve described by Eqs. (2) or (3), respectively, visualized in Fig. 1(c). These witnesses provide sufficient, but not necessary conditions. That is, if we are within the blue or green area, then we can definitely claim the NC or NG of the state. However, for example, if a point is above the NG boundary, the result is inconclusive: it might be either non-Gaussian or not.

Note that we do not have to know the exact value of the parametric gain G as these witnesses of NC and NG were derived for the asymptotic $G \to \infty$ limit, which implies a faithful witness for any finite value of G (see Supplemental Material [35], Sec. S.I).

Importantly, these witnesses were constructed for phase-independent states as this assumption simplifies both the theoretical formulation of the witness and its experimental realization (eliminating phase noise). Since our current scheme uses a heralded quasi-single photon as a signal, it is inherently phase-independent; thus, the assumption holds. Similar witnesses can also be constructed for the general case, but are outside of the scope of the current manuscript.

The gray dashed area in Fig. 1(c) cannot be reached by phase-independent states. That is, a measurement result in that area indicates the phase-dependence of the input state. For example, a weakly squeezed single photon state,

which is phase-dependent and non-Gaussian, can reach point ($\mu_{\text{rel}} = 2, g^{(2)} = 1.66$) within the gray dashed area in Fig. 1(c). The dashed line bounding this area corresponds to input mixtures of vacuum and single-photon states for $\mu_{\text{rel}} \in [1, 3)$ and to input mixtures of single- and two-photon states for $\mu_{\text{rel}} \in [3, 5)$, which are, of course, non-Gaussian.

A. Special case: A heralded quasi-single-photon state

For demonstration, we focus on the case of a quantum state obtained through single-photon heralding at the output of a weakly pumped two-mode squeezer. This state is a mixture of a vacuum, a single-photon state, and higher-order Fock states whose contributions are small ($p_{2+} \ll 1$). This heralded state is straightforward to model (see Supplemental Material [35], Sec. S.II), and all photon-number probabilities and moments are analytically accessible for a given set of input parameters (losses, mean number of photon pairs leaving the crystal). This scenario is therefore ideal to compare the performance of the coincidence- and moment-based witnesses.

IV. EXPERIMENT

We generate the heralded quasi-single-photon state from a twin-beam source and track its NG through optical parametric amplification while varying the source brightness. Higher brightness leads to increased multi-photon contributions, which in turn reduces the NG of the state. Figure 2 shows the experimental scheme. The source is pumped with 1 ps pulses at 400 nm and phase-matched for non-collinear degenerate type-II SPDC. The brightness of the source, i.e., the number of photons per pulse (ppp), is controlled by adjusting the input pump power. The idler beam is directed to a heralding SPD1, while the signal is fed into the OPA. The latter is a nonlinear crystal cut for type-I collinear degenerate phase matching and pumped with the same laser pulses but at higher power, leading to gain $G = 6.5 \pm 0.5$. To ensure single-mode detection, we use a 0.5-nm spectral filter (BP1,2) and a single-mode fiber (SMF1,2) in both heralding and detection channels. Finally, the photodetection (PD) is done with a camera. More details about the experimental setup, the source, and the OPA are presented in Appendix A.

A. Characterization of the source

We start by characterizing the source through the standard HBT coincidence measurement [14]. For this, we employ a three-fold coincidence scheme: a single-photon detector in the heralding channel (SPD1) triggers a coincidence circuit formed by two detectors (SPD2 and SPD3) in the signal arm. To measure the heralding efficiency, the coincidences between SPD1 and SPD2/SPD3 at 0 μs delay are detected [Fig. 2(i)]. The brightness of the source is set at 0.02 ppp, with the latter measured by SPD1 and evaluated at the source output. Side peaks at ±200 μs are caused by neighboring pulses and represent accidental coincidences. For this measurement, we use a 10-nm bandpass filter BP3 in the heralded arm, which ensures the detection of signal photons across all spectral

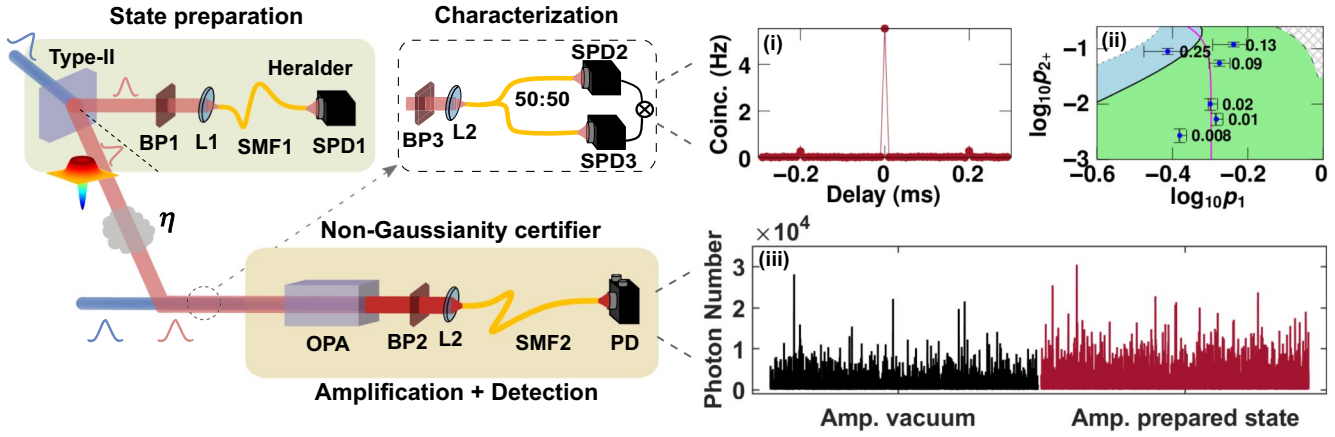


FIG. 2. Experimental scheme. Quantum states are prepared (green shaded box) through heralding on the idler photons of type-II SPDC using a single-photon detector (SPD1) after filtering with a bandpass filter (BP1) and a single-mode fiber (SMF1). For certification (yellow shaded box), heralded signal photons are fed into optical parametric amplifier OPA, whose output, after similar filtering with BP2 and SMF2, is registered by photodetector PD (a camera). The efficiency η includes both the detection and coupling into the OPA. The dashed box shows an HBT setup with single-photon detectors SPD2,3 used for the characterization of the heralded state. Inset (i) the histogram of coincidences between SPD1 and SPD2/SPD3 for the brightness of the source, measured by SPD1, set at 0.02 photons per pulse at the source output. Inset (ii) single- and multiphoton probabilities obtained for heralded states of varying brightness, quantified through the mean number of photons per pulse at the source output. The magenta line shows the analytic curve for the fixed heralding efficiency of 51%. Inset (iii) photon numbers for a sequence of 35000 pulses in the cases of vacuum (left) and heralded photon of brightness 0.12 photons per pulse (right) states at the input.

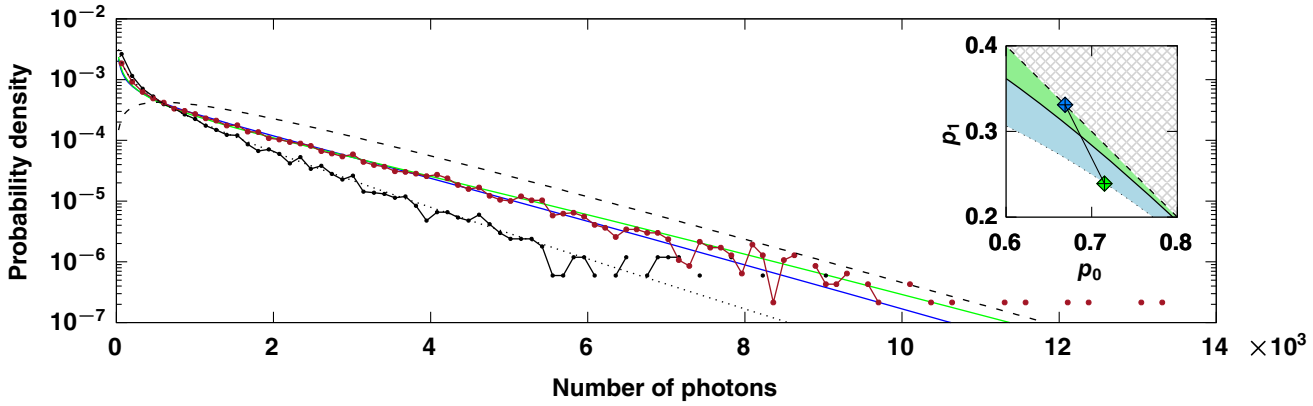


FIG. 3. Photon-number distributions of the amplified vacuum (black solid line) and amplified heralded state with a brightness of 0.12 photon per pulse (red solid line), measured over 35000 pulses. The dotted/dashed black line shows the theoretical photon-number distribution of amplified vacuum/ideally amplified single photon. The blue and green lines show the theoretical distributions for input states with $p_0 = 0.67$, $p_1 = 0.33$, $p_{2+} = 0$ (non-Gaussian) and $p_0 = 0.715$, $p_1 = 0.239$, $p_{2+} = 0.046$ (nonclassical), respectively. Inset: points corresponding to these states (blue and green crosses, respectively) in the (p_0, p_1) diagram.

modes. After correcting for the system optical transmissivity and SPDs' efficiencies, the heralding efficiency amounts to $\eta_H = 51 \pm 2\%$ (see Appendix C). This defines the purity of the heralded state at the input of the amplifier.

The rates of triggered coincidences between SPD2 and SPD3 provide the probabilities p_0, p_1, and p_{2+} (see Sec. Appendix E), from which the NG witness of the heralded state can be evaluated. Figure 2(ii) shows the obtained p_1 and p_{2+} values while varying the source brightness between 0.008 and 0.25 ppp. We see that the source features NG for brightness levels up to 0.13 ppp, but loses it as the brightness increases. The magenta line shows the theoretical values (see Supplemental Material [35], Sec. S.II) of p_1 and p_{2+} under a variable source brightness and a fixed $\eta_H = 51\%$, and aligns reasonably well with the experimental data.

B. Parametric amplification of the examined states

We now feed the examined states into the OPA and record photon numbers for 35000 pulses conditioned on detection events at SPD1. Figure 2(iii) shows an example of these records when the amplifier is seeded by vacuum (left) and by a heralded single-photon state with the brightness set at 0.12 ppp (right). In the latter case, the mean number of photons is clearly increased. Processing the data also shows that $g^{(2)}$ is reduced: while for amplified vacuum it is measured to be 3.00 ± 0.03, for the amplified heralded state it becomes 2.58 ± 0.03. This reduced value is, however, higher than the 1.66 expected for an amplified pure single-photon state [33]. Similarly, the mean photon number also increases insufficiently, resulting in $\mu_{\mathrm{rel}} = 1.66 \pm 0.02$ ($\mu = 946 \pm 6$ photons while $\mu_{\mathrm{vac}} = 570 \pm 7$ photons) instead of the expected value of 3. These discrepancies are caused by the reduced purity $\eta = \eta_H \eta_{\mathrm{OPA}}$ of the examined state, where η_{OPA} quantifies the efficiency of amplification and is primarily degraded by imperfect spectral/spatial mode matching between the input and amplifier modes (see Appendix B).

The corresponding intensity histograms $\mathcal{P}(N)$ are shown in Fig. 3 (for the derivation of the continuous approximations of the number distribution of squeezed Fock states, see Supplemental Material [35], Sec. S.III). The black dashed line presents the theoretical continuous approximation of the number distribution $\mathcal{P}_1(N)$ of an amplified pure single photon ($p_0 = p_{2+} = 0$, $p_1 = 1$), while the black dotted line shows the theoretical distribution $\mathcal{P}_0(N)$ of an amplified vacuum ($p_1 = p_{2+} = 0$, $p_0 = 1$) and it perfectly fits the corresponding experimental distribution (black solid line). The measured intensity histogram of the amplified heralded state is shown by a red solid line. As a mixture, this distribution can be approximated by $\mathcal{P}(N) = p_0\mathcal{P}_0(N) + p_1\mathcal{P}_1(N) + p_{2+}\mathcal{P}_2(N)$ (with $\mathcal{P}_2(N)$ denoting the approximate intensity distribution of a squeezed Fock-2 state), and it lies in between $\mathcal{P}_0(N)$ and $\mathcal{P}_1(N)$ for negligible p_{2+} values. To illustrate the impact of higher Fock contributions, we compare two distributions that yield the same experimental mean photon number. The blue line represents a pure vacuum-single-photon mixture ($p_0 = 0.67$, $p_1 = 0.33$, $p_{2+} = 0$), which is a non-Gaussian state by definition. The corresponding blue cross in p_0, p_1 space (inset in Fig. 3) sits precisely at the boundary between non-Gaussian and non-physical states. In contrast, the green solid line depicts a slightly more complex mixture including few higher Fock contributions ($p_0 = 0.715$, $p_1 = 0.239$, $p_{2+} = 0.046$). This state lies exactly on the NC boundary (green cross in the inset in Fig. 3). Despite describing very different states, the blue and green distributions both fit the experimental data reasonably well. This is mainly because the purity of the amplified state is degraded. This comparison highlights a key point: for low-purity states, non-Gaussianity is

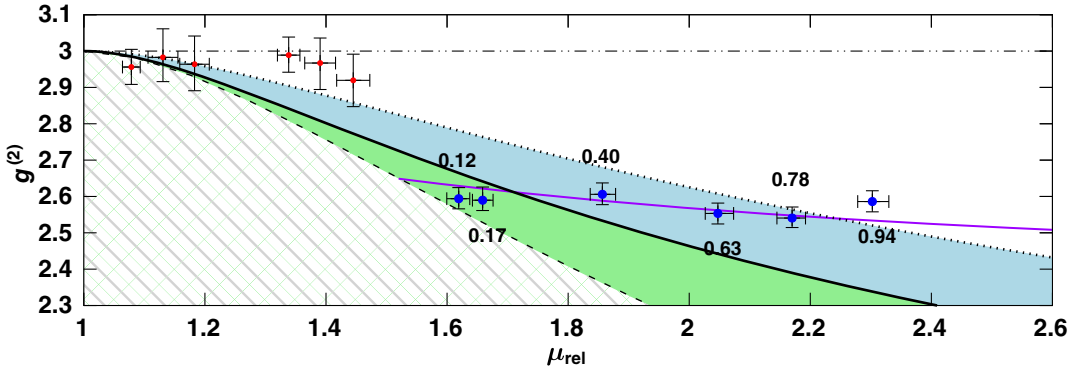


FIG. 4. Experimental post-amplification $g^{(2)}$ and relative mean photon numbers μ_{rel}. Blue circles correspond to heralded states for different source brightnesses, quantified through mean number of photons per pulse at the output. The blue and green areas correspond to the NC and NG witnesses from Fig. 1(c). The magenta line shows the dependence calculated analytically for a fixed effective transmittance of 26% while increasing the brightness of the source (from left to right). Red points show the results for a thermal state obtained from the same source without heralding. The measurement shows $g^{(2)}$ close to the theoretical value 3 (black dash-dotted line) and no nonclassicality.

non-trivial to certify through the post-amplification photon-number distribution.

On the other hand, the use of μ_{rel} and $g^{(2)}$ (Fig. 4) confirms the NG of states with low brightness, which are non-Gaussian according to the preliminary state characterization [Fig. 2(ii)]. The leftmost data point in Fig. 4, corresponding to the 0.12-ppp case, lies well within the NG region (green area). As the brightness of the input state increases (0.17, 0.40, 0.63, 0.78, 0.94 ppp), the contribution from higher-order Fock states becomes more significant, gradually pushing the measured $(\mu_{\mathrm{rel}}, g^{(2)})$ values out of the NG and then out of the NC region. The results are consistent with an overall transmissivity of $\eta = 26\%$ (magenta line). Given a heralding efficiency of 51%, this implies an amplification efficiency of $\eta_{\mathrm{OPA}} = 51\%$.

We also examined a set of thermal states (red points), obtained by measurements without conditioning on the events from SPD1. These states are Gaussian and classical. From left to right, the points correspond to the same source brightness levels as used in the conditional measurements. As expected, the points lie in the region where neither NG nor NC can be confirmed. The measured $(\mu_{\mathrm{rel}}, g^{(2)})$ values are close to $g^{(2)} = 3$ (black dash-dotted line).

We can now compare these new results with the ones of coincidence measurement. To this end, we convert both sets of data—probabilities p_1, p_0 on the one hand and $g^{(2)}, \mu_{\mathrm{rel}}$ on the other hand—to pre-amplification moments m, s^2 (rescaling the coincidence measurement to the average 26% effective transmittance obtained in Fig. 4). The result is shown in Fig. 5. We see that the two sets of points line up very well, and the points with similar mean numbers of photons lie close to each other. The measurement with amplification was mostly done on brighter states to demonstrate the broader applicability of the scheme.

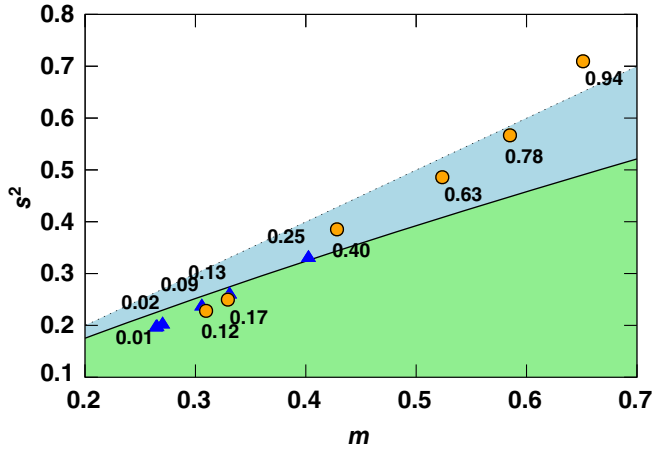


FIG. 5. Estimated photon-number mean and variance values before amplification from the coincidence measurement [blue triangles, see Fig. 2(ii)] and the values retrodicted from the amplified measurement (orange disks, cf. Fig. 4). The numeric values next to the symbols correspond to the mean number of photons per pulse at the source output. The solid black line shows the boundary of the non-Gaussianity witness, the dotted black line is the boundary of the nonclassicality (anti-bunching) witness, $s^2 = m$.

V. DISCUSSION

We have proposed and experimentally demonstrated optical parametric amplification as a tool for certifying the non-Gaussianity and nonclassicality of quantum states. Specifically, we theoretically showed that the directly measurable mean photon number and second-order correlation function after amplification provide information similar to that revealed from photon-number probabilities and coincidence measurements.

Experimentally, we examined a heralded quasi-single-photon state generated through spontaneous parametric

down-conversion and successfully tracked its transition from the non-Gaussian to the nonclassical and then to classical regime by increasing its brightness. We found that although the photon-number distributions of amplified Gaussian and non-Gaussian states are barely distinguishable, our proposed method allows us to accurately characterize these states. Furthermore, we showed that losses arising from the mismatch between the modes of the examined state and the amplifier do not affect this measurement. Moreover, we showed that post-amplification losses are irrelevant, as the measurement remained valid even under detection losses exceeding 99.5%, primarily due to spatial and spectral filtering. Our experimental results closely match the predictions of the developed theory and agree with the results obtained through the standard coincidence measurements. We stress that the single-photon detectors in our experiment had significantly higher detection efficiency, yet they provided similar performance.

In addition to eliminating the need for single-photon detectors, an OPA naturally enables multimode detection. This is especially important for applications where distinct non-Gaussian states occupying multiple modes need to be certified simultaneously. Thus, our method is an excellent candidate for high-dimensional quantum information technologies.

Importantly, the OPA-based non-Gaussianity and nonclassicality certification approach proposed and realized in the current manuscript turns out to be applicable in a broader context (higher-order Fock states, phase-dependent states, multimode states with independent modes, different principles of realization), which is proved and discussed by some of us in Ref. [31].

We note that a current, independent approach came to our attention, which also uses correlation functions to characterize the non-Gaussianity of states [36]. Similarly to the standard approach, they also use single-photon detectors, while our method only needs intensity detectors.

ACKNOWLEDGMENTS

The project is part of the Munich Quantum Valley, supported by the Bavarian state government with funds from the Hightech Agenda Bavaria. M. V. C. acknowledges funding from the Deutsche Forschungsgemeinschaft (DFG) under Grant No. 499995074. This research was funded within the QuantERA II Programme (project SPARQL), which received funding from the European Union's Horizon 2020 research and innovation programme under Grant Agreement No. 101017733. L. R. and E. R. acknowledge the Grant No. 23-06224S of the Czech Science Foundation. L. R., E. R. and R. F. acknowledge the European Union's HORIZON Research and Innovation Actions under Grant Agreement No. 101080173 (CLUSTEC), and the Quantera project CLUSSTAR (Grant No. 8C24003) of MEYS, Czech Republic. R. F. acknowledges the project LUC25006 of the MEYS of the Czech Republic. R. F. acknowledges discussions with Ch. Hotter and A. S. Sørensen, who independently derived quantum non-Gaussian criteria for correlation functions.

DATA AVAILABILITY

The data that support the findings of this article are available upon request.

APPENDIX A: DETAILED EXPERIMENTAL SCHEME

Figure 6 presents the complete experimental setup. After power control (PC) with a polarizing beam-splitter and a half-wave plate (HWP), another polarizing beam splitter (PBS) separates the pump beam (1 ps pulses at 400 nm at a 5-kHz repetition rate) into two arms. The pump power splitting ratio is controlled with a HWP. In the upper arm, the pump is focused to waist $w_p = 105$ μm onto a 3-mm thick beta barium borate (BBO) crystal, configured for beam-like [37,38] type-II SPDC, generating photon pairs at the degenerate wavelength of 800 nm. A variable neutral density (ND) filter is included to vary the brightness of the SPDC source by adjusting the pump power. The idler photons (H-polarized) are transmitted through the PBS and directed to the heralding arm. After collimation with lens F1 = 30 mm, the idler beam passes through a 0.5-nm interference filter centered at 800 nm to ensure spectral purity and is then coupled into a single-mode fiber (SMF) using lens F2 = 5.5 mm. The SMF guides the photons to a superconducting nanowire SPD with a quantum efficiency of approximately 80%. This detector acts as a heralding trigger, sending a signal to open the shutter of an sCMOS camera for synchronized detection of the amplified signal. The signal photons

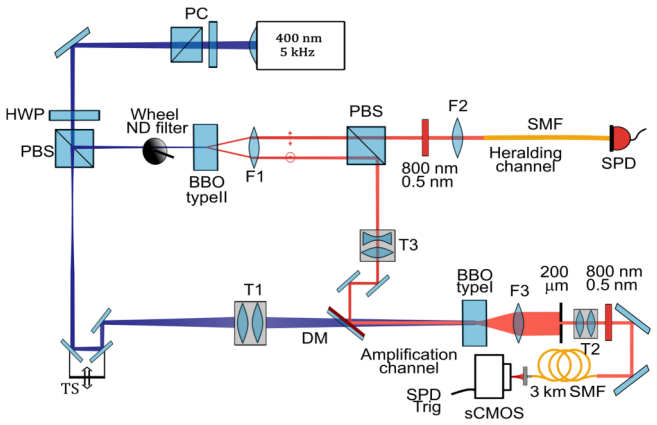


FIG. 6. Full experimental setup. HWP, half-wave plates; M1-4, mirrors; DM, dichroic mirror; PBS, polarizing beam splitter; ND, neutral density filter; F1-3, lenses; T1-3, telescopes; TS, translational stage; SM, spherical mirror; BBO, beta-barium borate; SMF, single mode fiber; sCMOS, scientific complementary metal-oxide-semiconductor camera.

(V-polarized), reflected by the PBS, are directed into the amplification arm.

The same laser source used for SPDC also pumps the OPA, which is a 3-mm-thick bismuth borate crystal under collinear degenerate type-I phase matching. The amplifier is operated in a phase-sensitive configuration with the parametric gain $G = 6.5 \pm 0.5$, optimized for high signal-to-noise ratio. To achieve spatial mode matching, telescopes T1 (−50 mm and 50 mm) and T3 (−30 mm and 75 mm) are employed. Temporal overlap between the signal and pump pulses is ensured using a translation stage (TS) in the pump path. The amplified signal is collimated by lens F3 = 75 mm and filtered: spatially, with a 200-μm pinhole, and spectrally, with a 0.5-nm interference filter similar to the one in the heralding arm. The amplified radiation is detected by an sCMOS camera whose quantum efficiency is approximately 50%. Upon receiving a trigger signal from the SPD, the camera requires ∼10 μs to start the exposure. To synchronize it with the heralding signal, the amplified beam is delayed by 15 μs using a 3-km SMF.

APPENDIX B: MODE MATCHING AND THE EFFICIENCY OF AMPLIFICATION

Mode matching is an important factor governing the efficiency of the OPA process. Indeed, for a single-mode field a_0 at the input of the OPA, the addressed state is $\hat{a} = \sqrt{\eta_{\mathrm{OPA}}}\hat{a}_0 + \sqrt{1-\eta_{\mathrm{OPA}}}\hat{a}_v$, where $\hat{a}_v$ is the vacuum field and η_{OPA} defines the mode overlap between the input and the amplifier mode. That is, if mode matching is imperfect ($\eta_{\mathrm{OPA}} < 1$), the efficiency of the amplification decreases because of the vacuum contribution. In our case, the heralded photon, generated using a type-II source, has a much narrower spectral mode (≈0.5 nm) when compared to the amplifier mode (≈9 nm) based on type-I collinear-degenerate phase matching. This is the main reason behind the degraded OPA efficiency, which amounts to $\eta_{\mathrm{OPA}} = 51\%$. However, this issue can be resolved by spectrally shaping the OPA modes. Alternatively, a broadband single-photon source based on type-I parametric down-conversion would suit the detection scheme.

On top of the loss-induced noises, there can be other types of noise in the system. However, the high-fidelity state reconstruction with a similar setup [28] indicates that the effect of such noises is small, mainly because the measured photon number is defined by the quadrature strongly amplified by the OPA. As the simplest example, let us consider an additive thermal noise (for instance, due to fluorescence from the OPA or other parasitic background processes) with mean $\bar{n}$ (and consequently variance $\bar{n}(\bar{n}+1)$) and look at how it changes the $g^{(2)}$ of amplified vacuum: $g^{(2)\prime} = 1 + \frac{2\cosh^2 G \sinh^2 G + \bar{n}(\bar{n}+1)}{[\sinh^2 G + \bar{n}]^2} - \frac{1}{[\sinh^2 G + \bar{n}]}$. For example, if $\bar{n} = 0.025\ \sinh^2 G$, i.e., 2.5% of the mean intensity of amplified vacuum, this results in $g^{(2)\prime} \approx 2.9$, which is significantly lower than the measured value of $g^{(2)}$ for amplified vacuum. Thus, in our experiment, the added noise will be negligible. In case of a larger effect, one can characterize the imperfection and correct for it.

APPENDIX C: HERALDING EFFICIENCY

The heralding efficiency η_H is defined as the probability to observe a photon in the signal arm, provided that a photon was detected in the heralding arm. If higher Fock-state probabilities are negligible, this quantity coincides with the single-photon probability p_1. For instance, setting the brightness of the source to 0.01 ppp, we had $6 \cdot 10^{-4}$ coincidences per pulse between SPD1 and SPD2, with $8 \cdot 10^{-3}$ clicks per pulse on the heralding arm SPD1. Correcting for 38% SPD2 efficiency, 50% beamsplitter, 90% optical transmissivity, and 85% fiber coupling, we obtained $\eta_H = 51 \pm 2\%$, and it corresponds to the purity of the prepared quasi-single-photon state. For higher source brightness, multiphoton effects start to play a significant role. Still, one can use the model described in Sec. S.II of the Supplemental Material [35] to evaluate the heralding efficiency, which provides similar numbers.

APPENDIX D: DETECTION LOSSES

From the gain of the amplifier, we can estimate the mean photon number of the amplified vacuum as $\mu'_{\mathrm{vac}} = \sinh^2(6.5)$. The measured value, however, is significantly lower: $\mu_{\mathrm{vac}} = 570$ photons. This large discrepancy is attributed to optical losses, amounting to $1 - \frac{\mu_{\mathrm{vac}}}{\mu'_{\mathrm{vac}}} \approx 99.5\%$, primarily caused by spatial and spectral filtering. The latter highlights the loss-tolerance of the presented scheme, as NG witness results were obtained despite the presence of such significant losses.

APPENDIX E: PHOTON-NUMBER PROBABILITIES FROM HBT MEASUREMENTS

Assuming that an incoming signal with unknown photon-number distribution is split on a beam splitter with transmittance T, and the transmitted photons are measured by detector A with probability p_A, whereas the reflected photons are detected by detector B with probability p_B, we can estimate the photon-number probabilities of a weak signal as

$$p_{2+} = \frac{Q_2}{2\, p_A p_B T R'}, \tag{E1}$$

$$p_1 = Q_1 - p_2\left[\frac{2TR\,(q_B p_A + q_A p_B) + T^2(1-q_A^2)}{T p_A + R p_B} + \frac{R^2(1-q_B^2)}{T p_A + R p_B}\right], \tag{E2}$$

$$p_0 = 1 - p_1 - p_{2+}, \tag{E3}$$

with Q_2 denoting the probability of double clicks and Q_1 denoting the probability of single clicks; $R \equiv 1-T$, $q_A \equiv 1-p_A$, and $q_B \equiv 1-p_B$ were introduced for convenience (for details on the derivation of these formulas, see Supplemental Material [35], Sec. S.IV). A similar approach was used in [14] to estimate Fock probabilities, the difference is that we also account for imperfect detection ($p_A \neq 1$ and $p_B \neq 1$).

Knowing the value of extra loss characterized by a transmittance T' and suffered before the beam splitter of the HBT scheme, it is straightforward to correct for it assuming a weak signal:

$$\begin{aligned} p'_{2+} &= \frac{p_{2+}}{T'^2}, \\ p'_1 &= \frac{p_1}{T'} - 2p'_{2+}(1-T'), \\ p'_0 &= 1 - p'_1 - p'_{2+}. \end{aligned}$$

These formulas were used to correct the HBT results for optical losses and fiber coupling losses in Fig. 2(c). Note that an alternative approach has been recently used in [39], where they include the loss directly into the witness.

APPENDIX F: NON-CLASSICALITY AND NON-GAUSSIANITY WITNESSES

The NG witness introduced in [14] can be expressed as a parametric curve [solid black line in Fig. 1(a)] parametrized by $r \geq 0$:

$$\begin{aligned} \tilde{p}_0(r) &= \frac{\exp\{-\frac{1}{4}(e^{4r}-1)(1-\tanh r)\}}{\cosh r}, \\ \tilde{p}_1(r) &= \frac{(e^{4r}-1)\exp\{-\frac{1}{4}(e^{4r}-1)(1-\tanh r)\}}{4\cosh^3 r}. \end{aligned} \tag{F1}$$

Any state for which the pair of zero-photon and single-photon probabilities lies beyond this curve [green area in Fig. 1(a)] cannot be represented as a mixture of Gaussian states. The nonclassicality witness in terms of number probabilities can be given simply as $p_1 > -p_0 \ln p_0$ [14] [area above the dotted line in Fig. 1(a)].

For our purposes, we are interested in the post-amplification witnesses for phase-independent input states. It is straightforward to show that for phase-independent states, the relationship between pre- and post-amplification moments can be written as (for more details, see Supplemental Material [35], Sec. S.I):

$$\begin{aligned} \mu &= \sinh^2 G + m\cosh 2G, \\ \sigma^2 &= s^2\frac{3\sinh^2 2G+2}{2} + (m^2+m+1)\frac{\sinh^2 2G}{2}. \end{aligned} \tag{F2}$$

For a fixed value of the parametric gain G, μ is an increasing linear function of m, and for fixed values of m and G, the value of σ^2 is an increasing linear function of s^2. Therefore, the problem of minimizing σ^2 for a fixed value of μ is equivalent to minimizing s^2 for a fixed value of m. The problem of minimizing s^2 over arbitrary mixtures of Gaussian states for a fixed value of m is proven in [31]; the NG boundary can be given in a parametric form as

$$\begin{aligned} m_{\mathrm{NG}}(r) &= \frac{e^{3r}}{4} - \frac{1}{2} + \frac{e^{-r}}{4}, \\ s^2_{\mathrm{NG}}(r) &= \frac{3e^{2r}}{8} - \frac{1}{2} + \frac{e^{-2r}}{8}, \end{aligned} \tag{F3}$$

where $r \geq 0$. This boundary is shown in Fig. 1(b) with a thick black line. Note that for a fixed m, the minimization of the variance s^2 is equivalent to minimizing the pre-amplification values of the second-order correlation function, the second moment of the integrated intensity, and the non-centered second moment of the photon numbers, so such alternatives can be used interchangeably. (Note that the latter is a convex function, and that form is used to prove the validity of witness for mixtures, for details, see [31]).

Using the relationship in Eq. (F2), the parametric boundary curve in Eq. (F3) can be transformed to its post-amplification form $\mu_{\mathrm{NG}}(r,G)$ and $\sigma^2_{\mathrm{NG}}(r,G)$. In order to handle scaling issues, we can express the post-amplification witness via the mean relative to that of the squeezed vacuum $\mu_{\mathrm{rel,NG}}(r,G) \equiv \mu_{\mathrm{NG}}(r,G)/\sinh^2 G$, and the second-order correlation function $g^{(2)}_{\mathrm{NG}}(r,G) \equiv 1 + \sigma^2_{\mathrm{NG}}(r)/\mu^2_{\mathrm{NG}}(r,G) - 1/\mu_{\mathrm{NG}}(r,G)$. It can be shown (see Supplemental Material [35], Sec. S.I) that for a fixed value of μ_{rel}, the $G \to \infty$ case provides the strictest condition on $g^{(2)}$ for witnessing quantum non-Gaussianity (i.e., the asymptotic witness is faithful for any finite value of G). Using this conservative $G \to \infty$ limit leads us to the following simplified boundary of the post-amplification non-Gaussianity witness:

$$\begin{aligned} \tilde{\mu}_{\mathrm{rel}}(r) &= e^r\cosh 2r, \\ \tilde{g}^{(2)}(r) &= 3 - 3\cdot\frac{\sinh^2 r\cdot(\sinh 2r+1)}{\cosh^2 2r}, \end{aligned} \tag{F4}$$

with $r \geq 0$. A state can thus be certified as quantum non-Gaussian if the pair of measured $(\mu_{\mathrm{rel}}, g^{(2)})$ values is located below the parametric curve defined by Eq. (F4) [i.e., below the thick black line in Fig. 1(c)]. Note that for large values of r, $\tilde{g}^{(2)}(r) \approx 3/2 + 9e^{-4r}$, whereas for small values, $\tilde{g}^{(2)}(r) \approx 3 - 3r^2$.

The nonclassicality witness in terms of $g^{(2)}$ and μ_{rel} is straightforward to calculate using that the photon number variance of a coherent state is equal to its mean ($s^2 = m$), and yields

$$g^{(2)} < \frac{3}{2} + \frac{3}{\mu_{\mathrm{rel}}} - \frac{3}{2\mu_{\mathrm{rel}}^2}. \tag{F5}$$

In their stated forms, the NC/QNG witnesses are valid only for a single mode. However, this assumption is close to the truth in our case, since the parametrically amplified scheme includes a single-mode fiber.

[1] R. Takagi and Q. Zhuang, *Convex resource theory of non-Gaussianity*, Phys. Rev. A **97**, 062337 (2018).

[2] M. Walschaers, *Non-Gaussian quantum states and where to find them*, PRX Quantum **2**, 030204 (2021).

[3] A. Kawasaki, R. Ide *et al.*, *Broadband generation and tomography of non-Gaussian states for ultra-fast optical quantum processors*, Nat. Commun. **15**, 9075 (2024).

[4] A. I. Lvovsky, P. Grangier *et al.*, *Production and applications of non-Gaussian quantum states of light*, arXiv:2006.16985.

[5] L. Podhora, *Quantum non-Gaussianity of multiphonon states of a single atom*, Phys. Rev. Lett. **129**, 013602 (2022).

[6] G. P. Teja, C. Kumar, Láš Lachman, and R. Filip, *Quantum non-Gaussian high Fock states of light pulses and their superpositions*, Phys. Rev. Res. **7**, 033272 (2025).

[7] J. Peřina, V. Michálek, and O. Haderka, *Higher-order sub-Poissonian-like nonclassical fields: Theoretical and experimental comparison*, Phys. Rev. A **96**, 033852 (2017).

[8] A. Kenfack and K. Życzkowski, *Negativity of the Wigner function as an indicator of non-classicality*, J. Opt. B **6**, 396 (2004).

[9] M. Walschaers, C. Fabre, V. Parigi, and N. Treps, *Entanglement and Wigner function negativity of multimode non-Gaussian states*, Phys. Rev. Lett. **119**, 183601 (2017).

[10] M. Endo, T. Nomura, T. Sonoyama, K. Takahashi, S. Takasu, D. Fukuda, T. Kashiwazaki, A. Inoue, T. Umeki, R. Nehra, P. Marek, R. Filip, K. Takase, W. Asavanant, and A. Furusawa, *High-rate four photon subtraction from squeezed vacuum: Preparing cat state for optical quantum computation*, arXiv:2502.08952.

[11] S. Konno, W. Asavanant, F. Hanamura, H. Nagayoshi, K. Fukui, A. Sakaguchi, R. Ide, F. China, M. Yabuno, S. Miki, H. Terai, K. Takase, M. Endo, P. Marek, R. Filip, P. van Loock, and A. Furusawa, *Logical states for fault-tolerant quantum computation with propagating light*, Science **383**, 289 (2024).

[12] V. Magro, J. Vaneecloo, S. Garcia, and A. Ourjoumtsev, *Deterministic freely propagating photonic qubits with negative Wigner functions*, Nat. Photonics **17**, 688 (2023).

[13] R. Filip and L. Mišta, *Detecting quantum states with a positive Wigner function beyond mixtures of Gaussian states*, Phys. Rev. Lett. **106**, 200401 (2011).

[14] M. Ježek, I. Straka, M. Mičuda, M. Dušek, Jír Fiurášek, and R. Filip, *Experimental test of the quantum Non-Gaussian character of a heralded single-photon state*, Phys. Rev. Lett. **107**, 213602 (2011).

[15] M. Ježek, A. Tipsmark, R. Dong, J. Fiurášek, L. Mišta, R. Filip, and U. L. Andersen, *Experimental test of the strongly nonclassical character of a noisy squeezed single-photon state*, Phys. Rev. A **86**, 043813 (2012).

[16] C. H. H. Schulte, J. Hansom, A. E. Jones, C. Matthiesen, C. Le Gall, and M. Atatüre, *Quadrature squeezed photons from a two-level system*, Nature (London) **525**, 222 (2015).

[17] M. G. Genoni, M. L. Palma, T. Tufarelli, S. Olivares, M. S. Kim, and M. G. A. Paris, *Detecting quantum non-Gaussianity via the Wigner function*, Phys. Rev. A **87**, 062104 (2013).

[18] J. Fiurášek, L. Lachman, and R. Filip, *Quantum non-Gaussianity criteria based on vacuum probabilities of original and attenuated state*, New J. Phys. **23**, 073005 (2021).

[19] J. Fiurášek, *Certification of stellar ranks of quantum states of light with a pair of click detectors*, Phys. Rev. A **112**, 063712 (2025).

[20] R. Filip and L. Lachman, *Hierarchy of feasible nonclassicality criteria for sources of photons*, Phys. Rev. A **88**, 043827 (2013).

[21] L. Lachman and R. Filip, *Robustness of quantum nonclassicality and non-Gaussianity of single-photon states in attenuating channels*, Phys. Rev. A **88**, 063841 (2013).

[22] K. Bencheikh, O. Lopez, I. Abram, and J. A. Levenson, *Improvement of photodetection quantum efficiency by noiseless optical preamplification*, Appl. Phys. Lett. **66**, 399 (1995).

[23] E. Sendonaris, J. Williams, R. Nehra, R. Gray, R. Sekine, L. Ledezma, and A. Marandi, *Ultrafast single-photon detection using nanophotonic parametric amplifiers*, Phys. Rev. Appl. **25**, 044078 (2026).

[24] U. Leonhardt and H. Paul, *High-accuracy optical homodyne detection with low-efficiency detectors: "Preamplification" from antisqueezing*, Phys. Rev. Lett. **72**, 4086 (1994).

[25] Y. Shaked, Y. Michael, R. Z. Vered, L. Bello, M. Rosenbluh, and A. Pe'er, *Lifting the bandwidth limit of optical homodyne measurement with broadband parametric amplification*, Nat. Commun. **9**, 609 (2018).

[26] G. Frascella, E. E. Mikhailov, N. Takanashi, R. V. Zakharov, O. V. Tikhonova, and M. V. Chekhova, *Wide-field SU(1,1) interferometer*, Optica **6**, 1233 (2019).

[27] R. Nehra, R. Sekine, L. Ledezma, Q. Guo, R. M. Gray, A. Roy, and A. Marandi, *Few-cycle vacuum squeezing in nanophotonics*, Science **377**, 1333 (2022).

[28] M. Kalash and M. V. Chekhova, *Wigner function tomography via optical parametric amplification*, Optica **10**, 1142 (2023).

[29] É. Rácz, L. Ruppert, and R. Filip, *OPA tomography of non-Gaussian states of light*, Quantum Sci. Technol. **9**, 045054 (2024).

[30] I. Barakat, M. Kalash, D. Scharwald, P. Sharapova, N. Lindlein, and M. Chekhova, *Simultaneous measurement of multimode squeezing through multimode phase-sensitive amplification*, Opt. Quantum **3**, 36 (2025).

[31] É. Rácz, L. Ruppert, and R. Filip, *Witnessing quantum non-Gaussianity from intensity moments*, arXiv:2509.20492.

[32] R. J. Glauber, *The quantum theory of optical coherence*, Phys. Rev. **130**, 2529 (1963).

[33] M. S. Kim, F. A. M. de Oliveira, and P. L. Knight, *Properties of squeezed number states and squeezed thermal states*, Phys. Rev. A **40**, 2494 (1989).

[34] L. Mandel and E. Wolf, *Optical Coherence and Quantum Optics* (Cambridge University Press, Cambridge, England, 1995).

[35] See Supplemental Material at http://link.aps.org/supplemental/10.1103/j68x-skmn for detailed theoretical analysis.

[36] C. Hotter, C. Henke, C. J. van Diepen, P. Lodahl, and A. S. Sørensen, *A quantum non-Gaussianity criterion based on photon correlations* $g^{(2)}$ *and* $g^{(3)}$, arXiv:2511.08488.

[37] C. Kurtsiefer, M. Oberparleiter *et al.*, *Generation of correlated photon pairs in type-II parametric down conversion—revisited*, J. Mod. Opt. **48**, 1997 (2001).

[38] S. Takeuchi, *Beamlike twin-photon generation by use of type II parametric downconversion*, Opt. Lett. **26**, 843 (2001).

[39] R. Checchinato, J.-H. Littmann, L. Lachman, J. Lee, S. Höfling, C. Schneider, R. Filip, and A. Predojević, *Loss-resistant verification of quantum non-Gaussian photon statistics*, Phys. Rev. Res. **7**, 043097 (2025).